

# The role of a low-level jet for stirring the stable atmospheric surface layer in the Arctic

Ulrike Egerer<sup>1, now at <sup>3</sup></sup>, Holger Siebert<sup>1</sup>, Olaf Hellmuth<sup>1</sup>, and Lise Lotte Sørensen<sup>2</sup>

<sup>1</sup>Leibniz Institute for Tropospheric Research, Permoserstr. 15, 04318 Leipzig, Germany

<sup>2</sup>Aarhus University, Frederiksborgvej 399, 4000 Roskilde, Denmark

<sup>3</sup>National Renewable Energy Laboratory (NREL), 15013 Denver W Parkway, Golden, CO 80401, USA

**Correspondence:** Ulrike Egerer (ulrike.egerer@nrel.gov)

**Abstract.** In this study, we analyze the transition of a stable atmospheric boundary layer (ABL) with a low-level jet (LLJ) to a traditional stable ABL with a classic Ekman helix in the late-winter central Arctic. Vertical profiles in the ABL were measured with a hot-wire anemometer on a tethered balloon during a 15 h period in March 2018 in northeast Greenland. The tethered balloon allows high-resolution turbulence observations from the ground to the top of the ABL. The core of the LLJ was observed at about 150 m altitude, and its height and strength were associated with the temperature inversion. Increased turbulence was observed in the vicinity of the LLJ, but most of the turbulence does not reach down to the surface, thus decoupling the LLJ from the surface. Only when the LLJ collapses and the ABL again exhibits a more classical Ekman spiral, a coupling to the surface is re-established. The LLJ might enhance both advective and turbulent vertical transport of passive tracers such as aerosol particles or moisture in the often stably stratified Arctic ABL.

## 10 1 Introduction

Low-level jets (LLJs) are vertically more or less bounded wind fields with local maximum wind velocities exceeding the geostrophic wind. An LLJ, especially in conjunction with stably stratified boundary layers, is usually found in the upper region of the ABL or even partly just inside or above the inversion. LLJs are often related to inertia oscillations and a decoupling of the flow dynamics from the surface-layer friction (Blackadar, 1957; Smedman et al., 1993). There is a lively debate about the origin of LLJs (Vihma et al., 2011; Jakobson et al., 2013; Tuononen et al., 2015; Guest et al., 2018; Chechin and Lüpkes, 2019) and details of the mechanism behind this are still not completely understood. Polar regions are preferable locations for the occurrence of LLJs (Tuononen et al., 2015; López-García et al., 2022) due to frequently observed (extremely) stably stratified and shallow ABLs, in particular during cloudless (wintertime) conditions with strongly negative thermal-infrared net irradiance. In northeast coastal Greenland, the area of interest for this study, LLJs occur 60-70% of the time, are observed at very low altitudes and are attributed to katabatic flows (Tuononen et al., 2015).

The stably stratified boundary layer, as defined by an increase of potential temperature with height, usually exhibits comparably low turbulence. When neglecting cloud-related effects such as radiative cooling at cloud top, the only significant source of turbulent kinetic energy (TKE) is the surface roughness. However, due to the strong local wind shear below and above the wind maximum, an LLJ can introduce a significant amount of TKE (Smedman et al., 1993) and modulate the vertical distribution

25 of TKE (Jakobson et al., 2013; Banta et al., 2006). These wind shear zones are usually considered a source of TKE production as long as the damping effect of the inversion is not dominating over the TKE production. Boundary-layer flows with a source of turbulence at the top of the inversion generated by vertical wind shear have also been referred to as "upside down" (Mahrt, 1999). The relative importance of turbulence-generating wind shear and damping inversion is quantified by the dimensionless Richardson number ( $Ri$ ) defined later on. In addition to TKE production, LLJs may play an important role in the advection of  
30 momentum, turbulence, as well as aerosol particles and precursor gases (Stensrud, 1996; Algarra et al., 2019).

Here, we study the ABL evolution in terms of an LLJ, as observed by a set of subsequent vertical wind and temperature profiles measured with a tethered balloon in the framework of the Polar Airborne Measurements and Arctic Regional Climate Model SIMulation Project (PAMARCMiP) at Station Nord in northeast Greenland. The central question of this work is how the LLJ might affect the vertical distribution of turbulence and whether increased turbulence is observed at the surface when  
35 the LLJ occurs or collapses. This could indicate that properties advected with the LLJ, such as increased aerosol concentration or precursor gases, could also be mixed down to the surface after being advected over a certain distance inside the LLJ.

## 2 Observations

### 2.1 PAMARCMiP campaign

The PAMARCMiP field campaign was conducted at the Villum Research Station (VRS) on the military outpost 'Station Nord' in the northeast corner of Greenland on the small peninsula of Princess Ingeborg ( $81^\circ 36'N$ ,  $16^\circ 40'W$ ). Balloon observations  
40 were made from 10 March to 7 April 2018 about 2 km south of VRS at a small observation hut ('Flygers Hut') to minimize the station's influence. The site is located on the coastline between the Greenland Ice Sheet to the south and the Arctic Ocean, which is covered with sea ice for most of the year at this location. A glacier is located about 20 km to the south.

The LLJ and ABL structure observations are mainly based on the tethered balloon system BELUGA (Egerer et al., 2019a).  
45 Continuously running meteorological measurements at 9 m altitude at the VRS and three-dimensional wind data from an ultrasonic anemometer (USA-1, manufactured by METEK GmbH, Germany) mounted on a tower at 65 m height, support the analysis of the profile measurements.

### 2.2 The BELUGA setup

BELUGA is a modular system consisting of tethered balloons of various sizes and a variety of sensor packages. During  
50 PAMARCMiP, a  $9\text{ m}^3$  balloon with a maximum payload of 3 kg was used with multiple sensor packages. The instrument packages were deployed in a rotating sequence aboard BELUGA to ensure adherence to the payload limit; a flight overview table with deployed instruments is provided in Egerer et al. (2019b). In this work, data from two sensor packages are used: (i) A turbulence probe based essentially on a single-component hot-wire anemometer measuring wind speed with a sampling frequency of 500 Hz. A Pitot-static tube served as a reference for the hot-wire sensors. Fast temperature measurements were  
55 made with a cold-wire sensor. In addition to a calibrated thermometer as a reference for the cold-wire sensor, the data logger

provided additional pressure measurements for barometric altitude. (ii) A standard meteorological probe ("StdMeteo") based on a Graw DFM-09 radiosonde with an additional Pitot-static probe provided wind speed and direction using a compass. This package measured wind, temperature, and relative humidity at a frequency of 1 Hz and was intended for regular use on all flights. The absolute accuracy of the wind speed measurement with the Pitot-static tube is determined by the accuracy of the differential pressure sensor and is additionally inversely proportional to the wind speed itself. For typical wind speeds of  $5 \text{ m s}^{-1}$ , the absolute accuracy is only in the range of  $0.5 \text{ m s}^{-1}$  which is essentially noticeable by a zero offset and can therefore be partially corrected; however, the relative resolution is higher by a factor of 10 for the Pitot-static tube and the spectrally determined resolution of the hot-wire anemometer is in the range of  $0.2 \text{ cm s}^{-1}$  (Egerer et al., 2019a).

### 2.3 Measurements and synoptical situation

This study focuses on nine subsequent flights between 10:00 UTC on 29 March and 1:00 UTC on 30 March 2018, during the transition between polar night and day. The period was mainly characterized by the persistent occurrence of an LLJ, followed by a transition to a more classic stable ABL which is characterized by the wind speed increasing mostly logarithmically from the ground with height. The turbulence is generated by the wind shear and is therefore strongest near the ground and decreases continuously with height, depending on the damping effect of the temperature inversion. Synoptic conditions during this period were influenced by high air pressure over central Greenland yielding calm weather conditions at ground level. All flights occurred under cloudless conditions with only thin clouds well above 1000 m. Therefore, possible icing was not an issue.

Figure 1 provides an overview of the nine BELUGA flight profiles up to altitudes of 600 to 1400 m in combination with near-surface measurements. The near-surface conditions are quite variable in terms of temperature  $T$  and specific humidity  $q$ , with  $T$  ranging between  $-35 \text{ }^\circ\text{C}$  and  $-26 \text{ }^\circ\text{C}$  and  $q$  ranging between  $0.15$  to  $0.3 \text{ g kg}^{-1}$ . Qualitatively, there is an obvious high correlation between  $T$  and  $q$ . Wind speeds  $u$  were below  $2 \text{ m s}^{-1}$  and decreased towards the end of the observation period. The wind direction  $dd$  is mainly from the west, but turns over south to north from 16:00 UTC and back to west after 19:00 UTC. Between 13:00 and 14:00 UTC,  $T$  and  $q$  drop abruptly by  $-8 \text{ K}$  and  $0.2 \text{ g kg}^{-1}$ , respectively, along with a change in wind direction (southeast to north) and reach their previous values about one hour later.

## 3 Data analysis methods

In this study, we use the balloon-borne vertical profiles to relate the properties of an LLJ to the vertical structure of stability and turbulence. The literature reveals various definitions of an LLJ, mostly based on a local low-altitude wind velocity maximum greater than around  $2 \text{ m s}^{-1}$  (Tuononen et al., 2015; Andreas et al., 2000; Blackadar, 1957). We adopt and slightly modify this definition and define the following criteria for an LLJ: (i) the wind velocity maximum occurs below 250 m altitude and (ii) the difference between the maximum wind velocity in the LLJ core  $u_{\text{LLJ}}$  and the wind minimum  $u_{\text{min}}$  above and below (commonly the near-surface wind velocity) exceeds  $2.5 \text{ m s}^{-1}$ . The LLJ strength is then defined as  $\Delta u = u_{\text{LLJ}} - u_{\text{min}}$  with  $u_{\text{min}}$  being the higher value either above or below the jet core. The height of the LLJ core  $z_{\text{LLJ}}$  is typically located at the maximum height of

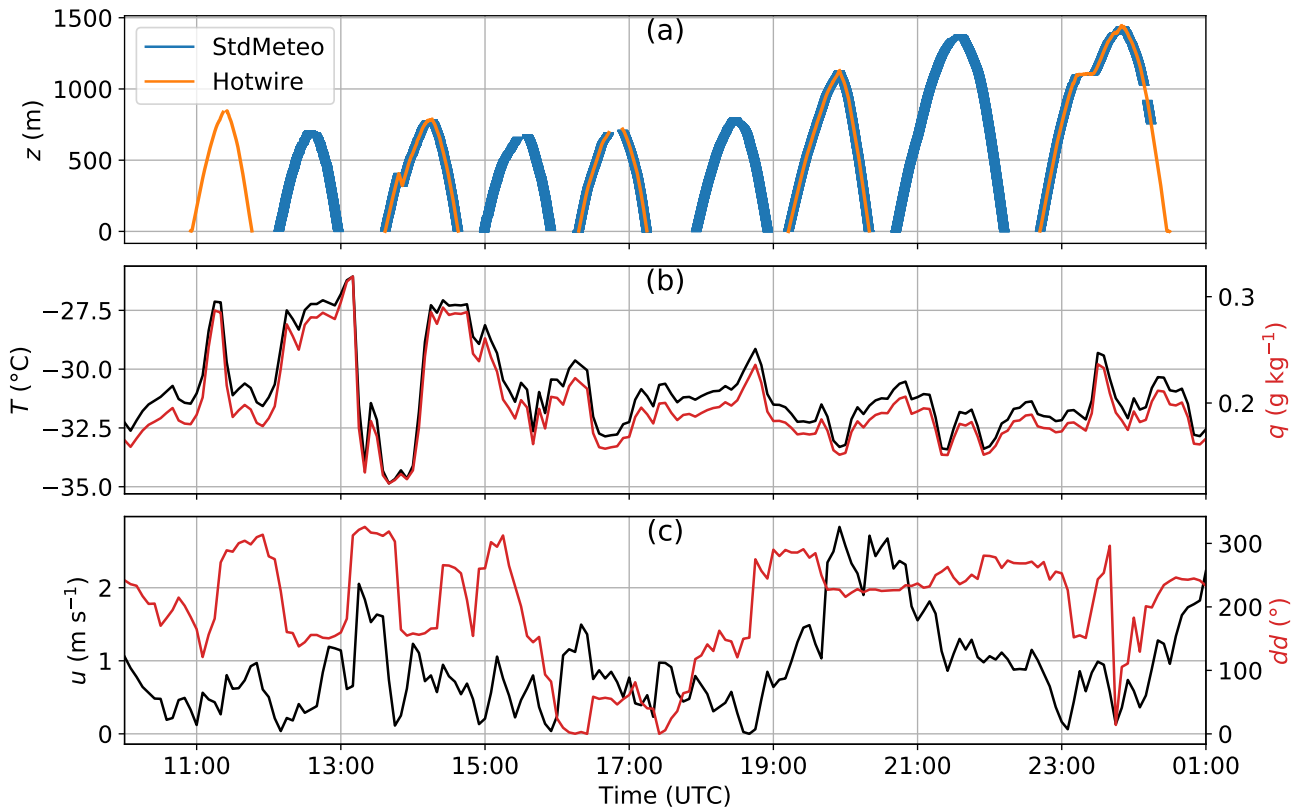


**Figure 1.** Time series for 29/30 March 2018 of (a) BELUGA flight altitude from the two instrument packages "StdMeteo" and "Hotwire" and (b) VRS near-surface measurements of temperature  $T$  and specific humidity  $q$  as well as (c) wind velocity  $u$  and wind direction  $dd$ .

the (strong) temperature inversion  $z_i$ . We tailor some of the criteria used in the literature to our specific observations and the unique characteristics of this particular LLJ.

90 The dimensionless gradient Richardson number  $\text{Ri}_g$  is the ratio of buoyancy to shear:

$$\text{Ri}_g = \frac{g}{\theta} \cdot \frac{\partial\theta/\partial z}{(\partial u/\partial z)^2}, \quad (1)$$

with the vertical gradient of the mean flow speed  $(\partial u/\partial z)^2 \approx (\partial u_x/\partial z)^2 + (\partial u_y/\partial z)^2$ , the vertical potential temperature gradient  $\partial\theta/\partial z$ , and the acceleration of gravity  $g$ . When stratification dominates over wind shear and a critical Richardson number  $\text{Ri}_c$  - estimated to be between 0.25 and 1 (Miles, 1961; Abarbanel et al., 1984) - is reached, turbulence decreases.

95 Thus, the contribution of buoyancy and shear to the turbulence profile throughout the ABL can be analyzed by the shear and buoyancy terms of the  $\text{Ri}_g$ . For estimating  $\text{Ri}_g$ ,  $u$  and  $\theta$  profiles are smoothed with a 10 s rolling mean before calculating the local gradients. The final  $\text{Ri}_g$  profile is then smoothed again with a rolling mean with a 10 s window. As an approximation for the range between the surface and the core of the LLJ, the bulk Richardson number  $\text{Ri}_b$  (Mahrt, 1985) is calculated for the

height  $z$ :

$$100 \quad \text{Ri}_b(z) = \frac{g}{\theta} \cdot \frac{\Delta\theta(z) \cdot z}{(\Delta u(z))^2}. \quad (2)$$

Here,  $\Delta\theta(z)$ , or  $\Delta u(z)$ , is the difference between  $\theta$ , or  $u$ , at  $z$  and close to the surface.

The local turbulence is characterized by means of the local energy dissipation rate  $\varepsilon$  which is derived from the second-order structure function of  $u$  applying inertial sub-range scaling:

$$\overline{(u(t-t^*) - u(t))^2} = C \cdot \varepsilon^{2/3} \cdot (t^* \cdot \bar{u})^{2/3} \quad (3)$$

105 with  $C = 2$  and a time lag  $t^*$  for the longitudinal wind velocity  $u$  (Siebert et al., 2006, Eq. 10 and 11; ). Here, the overline in Eq. (3) denotes time averaging; an averaging interval of 2 s was selected which yields robust estimates (Egerer et al., 2019a). The minimum resolvable  $\varepsilon$  is estimated to be about  $10^{-6} \text{ m}^2 \text{ s}^{-3}$ .

To better classify both the integration and averaging times in the determination of parameters as discussed before, but also to better interpret the vertical profiles in the next sections, knowledge of the length scales involved is of certain interest. Integral  
110 length scales of a turbulent flow, describing the size of the largest energy-containing eddies, can be defined according to

$$\mathcal{L} = \beta \cdot \sigma_u^3 / \varepsilon \quad (4)$$

(p. 16; Wyngaard, 2010) with a constant  $\beta$  of  $\mathcal{O}(1)$ . We call the ratio of individual, locally-fluctuating  $\frac{\sigma_u^3}{\varepsilon}$  values "local length scales"  $\mathcal{L}$ . Here,  $\varepsilon$  is interpreted as a local parameter derived from 30 s-long sub-records to be consistent with  $\sigma_u^3$  (with  $\sigma_u$  being the standard deviation of  $u$ ) averaged over 30 s, since  $\sigma_u$  is determined by the largest contributing scales. Earlier studies  
115 (Egerer et al., 2019a; Siebert et al., 2006) have shown that the estimation of dissipation rates is insensitive to the choice of the averaging time. Figure 2 shows a scatter plot of  $\varepsilon$  versus  $\sigma_u^3$  based on all BELUGA data observed on 29 March 2018. For each measuring point, the corresponding  $\text{Ri}_g$  value is represented by a color code to better classify the values. The relation of observed  $\varepsilon$  and  $\sigma_u^3$  is almost linear as predicted by Eq. (4), but shows some variations. A majority of resulting local length scales (98 % of the data points, assuming  $\beta = 1$ ) are in the range between 0.1 to 10 m with somewhat larger  $\mathcal{L}$  in regions of  
120 comparably high turbulence (blue-purple colors). A few data points with  $\text{Ri}_g > 1$  (yellow color) indicate small length scales below around 1 m. The ratio of the assumed mean wind velocity of  $\bar{u} \approx 5 \text{ m s}^{-1}$  to the averaging time of 30 s for estimating  $\sigma_u$  yields an averaging length of 150 m which is about 10 to 100 times larger than the  $\mathcal{L}$  estimates. Therefore, we can safely conclude that the averaging period covers enough eddies and the results are statistically robust.

For the 65 m mast wind data,  $\varepsilon$  is estimated analogously to the vertical profiles, but averaged over 5 min segments and using  
125 the vertical wind velocity component. The vertical wind velocity of the 65 m mast sonic anemometer for the flux calculation is tilt-corrected using the double-rotation algorithm described by Wilczak et al. (2001). For the determination of the turbulent fluxes of virtual sensible heat,  $H = \rho \cdot c_p \cdot \overline{\theta'_v w'}$ , and momentum,  $\tau_u = \rho \cdot \overline{u' w'}$ , the fluctuations are calculated by applying linear detrending and averaging over 30 min periods at 5 min time steps.

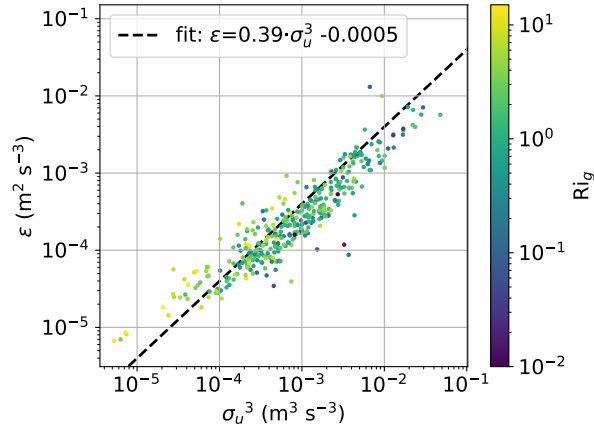


**Figure 2.** Relation of turbulence parameters for all BELUGA flights on 29 March 2018 with the hot-wire: Gradient Richardson Number  $Ri_g$ ,  $\sigma_u^3$ , and local dissipation rate  $\varepsilon$ . Each dot represents a 30 s time interval of averaged parameters. The dashed line shows a linear regression fitted to the data points.

## 4 Observed vertical structure of the ABL and LLJ

### 130 4.1 Evolution of the LLJ and ABL structure

We first analyze the evolution of the mean ABL structure and the LLJ throughout the observation period. Figure 3 provides an overview of the period based on BELUGA profiles (time-height contour plots), VRS observations in terms of meteorological measurements at 9 m and the sonic data at 65 m height. The observation period can be divided into three sub-periods: (I) an LLJ period, (II) a transition period, and (III) a standard stable ABL. By a "standard stable ABL" we refer to a cloud-free, shallow  
 135 stable ABL in which terrestrial radiation causes a surface-based temperature inversion, comparable to a nocturnal boundary layer at mid-latitudes.

In the first period (10:00 to 16:00 UTC), a clear LLJ emerges with a wind velocity maximum of about  $10 \text{ m s}^{-1}$  in a height of around 100 to 150 m, while the wind velocity in the near-surface layer remains below  $2 \text{ m s}^{-1}$ . The wind direction in the lower 400 m is west to northwest with the highest variability at surface level. A very stable surface layer develops with near-surface  
 140 temperatures around  $-30 \text{ }^\circ\text{C}$ , which increase by 10 K to 100 m height. The sharp surface temperature drop at 13:15 is not obvious at 65 m altitude and qualitatively correlates with a wind rotation to the north.

Between about 16:30 and 21:00 UTC, the wind velocity becomes more constant with height but generally decreases throughout the profile from about  $5 \text{ m s}^{-1}$  to less than  $2 \text{ m s}^{-1}$  with a highly variable wind direction. The LLJ disappears almost completely, and the strong surface temperature inversion now extends only to the lowermost tens of meters. At 17:00, however,  
 145 another smaller LLJ occurs with a maximum at a lower altitude compared to the previous LLJs of the first period. The temper-

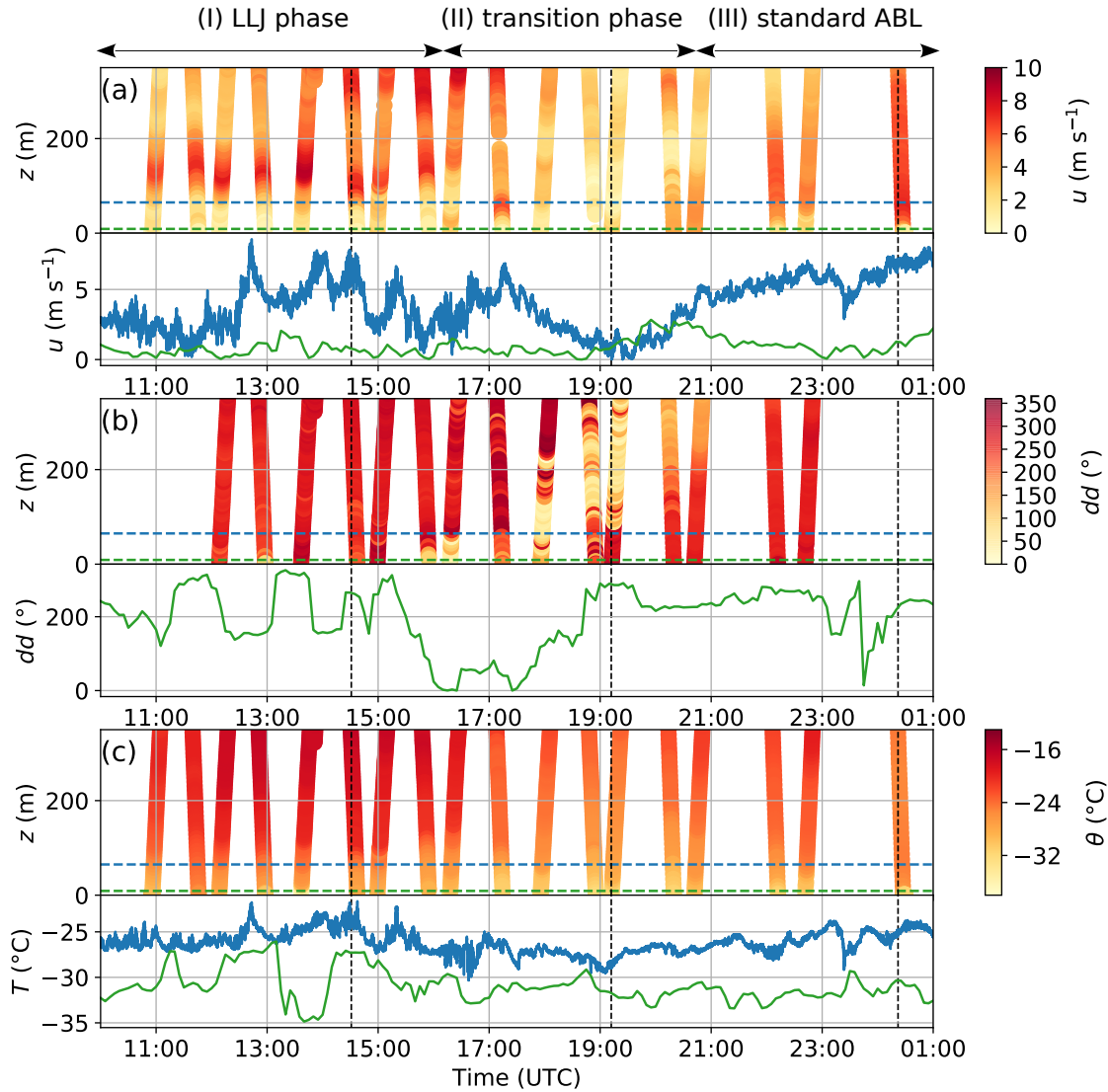


**Figure 3.** Time-height contour plots and time series observed at 9 m (green) and 65 m (blue) altitude for (a) wind velocity  $u$ , (b) wind direction  $dd$ , and (c) temperature  $T$  or potential temperature  $\theta$ . The data are from three different sources: (i) The time-height profiles are from BELUGA, (ii) the data shown at 9 m altitude are from VRS, and (iii) the data at 65 m altitude are from the mast. The dashed vertical lines represent the time of the example flights in Fig. 4.

ature throughout the entire profile decreases by about 5 to 10 K. This period is labeled as a transition between the LLJ period and a standard stable ABL structure.

After 21:00 UTC, the wind velocity increases with a local maximum at around 100 m but is much less pronounced compared to the LLJ structure observed in the first period. The wind direction is almost constant throughout the profile. The temperature profile is similar to the transition phase with a temperature inversion situated at a lower altitude.

For a more detailed analysis of the stratification during the three periods, four selected individual profiles of  $u$ ,  $\theta$ , and  $\varepsilon$  are plotted in Fig. 4. A well-developed LLJ is observed at 14:31 UTC. The wind velocity maximum of  $9 \text{ m s}^{-1}$  in 100 m coincides with the top of the strong surface-based temperature inversion. Above this inversion, the ABL is almost adiabatically stratified up to 150 m - the region with decreasing wind velocity. This region between 100 m and 150 m shows the highest local variability of wind velocity, although the wind shear is lower compared to the height range between 40 m and 100 m. This observation is visible in the local energy dissipation, which is highest - apart from the lowermost surface layer - in the upper part of the LLJ. Here, with almost neutral stratification, the wind shear term in Eq. (1) dominates the buoyancy term by one order of magnitude. Below the LLJ core in 40 to 100 m, the turbulence generation due to wind shear is reduced (compared to above the LLJ) by the influence of the temperature inversion. A local minimum of  $\varepsilon$  is located between the surface and the base of the LLJ, where the damping effect of the strong temperature inversion coincides with a height-constant wind velocity. Above 160 m,  $\theta$  again slightly increases with height and  $\varepsilon$  drops by two orders of magnitude.

The profile observed at 19:12 UTC in the transition phase shows the lowest wind velocity ( $\approx 1 \text{ m s}^{-1}$ ) between 50 m and 160 m. The maximum wind velocity is above  $3 \text{ m s}^{-1}$  in the near-surface layer, coinciding with a temperature inversion up to 40 m. However, just above this inversion, there is a shallow, 20 m-thick layer where the wind shear is strong enough to develop some turbulence indicated by a local maximum of  $\varepsilon$  up to  $10^{-3} \text{ m}^2 \text{ s}^{-3}$ . Above and below this maximum, stable stratification in combination with weak wind shear results in reduced turbulence. In the transition phase, one single profile includes an LLJ again, with a slightly different structure than the first period observations (Fig. 4, upper right). Here, the wind velocity increases with height directly above the surface with  $u_{\text{LLJ}} = 7 \text{ m s}^{-1}$  at 60 m height. The lowermost 20 m are neutrally stratified followed by a temperature inversion at  $z_i = 100 \text{ m}$ , which coincides with the wind minimum above the LLJ. Here, the  $\varepsilon$  profile is different from the LLJ cases, with maximum turbulence at the surface, gradually decreasing towards the upper bound of the LLJ, allowing turbulent mixing between the surface and the LLJ core. The upper part of the LLJ is still located inside the temperature inversion, leading to less turbulence in that region than for the LLJ phase. Above the LLJ, the turbulence intensity remains low and slightly increases at higher altitudes, with the wind velocity increasing again.

In the period with a standard stable ABL structure, the surface layer up to 50 m shows the largest increase of  $u$  and  $\theta$ , thus resulting in generally low values of  $\varepsilon$  compared to the previous periods. Above 50 m, the ABL is slightly stably stratified with an almost height-constant wind velocity, weakest turbulence at the top of the surface inversion, and some variable turbulence at higher altitudes. Throughout the profile, the values for buoyancy and shear increase or decrease to a similar degree, resulting in turbulence predominantly induced by surface roughness.

As a next step, we examine the temporal evolution of LLJ and ABL parameters. Figure 5 shows the time series of LLJ and temperature inversion strength and height, as well as  $\text{Ri}_b$  between surface and  $z_i$  derived from the profiles, combined with continuously measured turbulence parameters at 65 m. Except for a few cases in the transition phase, the LLJ strength correlates with the temperature inversion strength (Pearson correlation coefficient  $R = 0.52$ ). The LLJ height correlates even



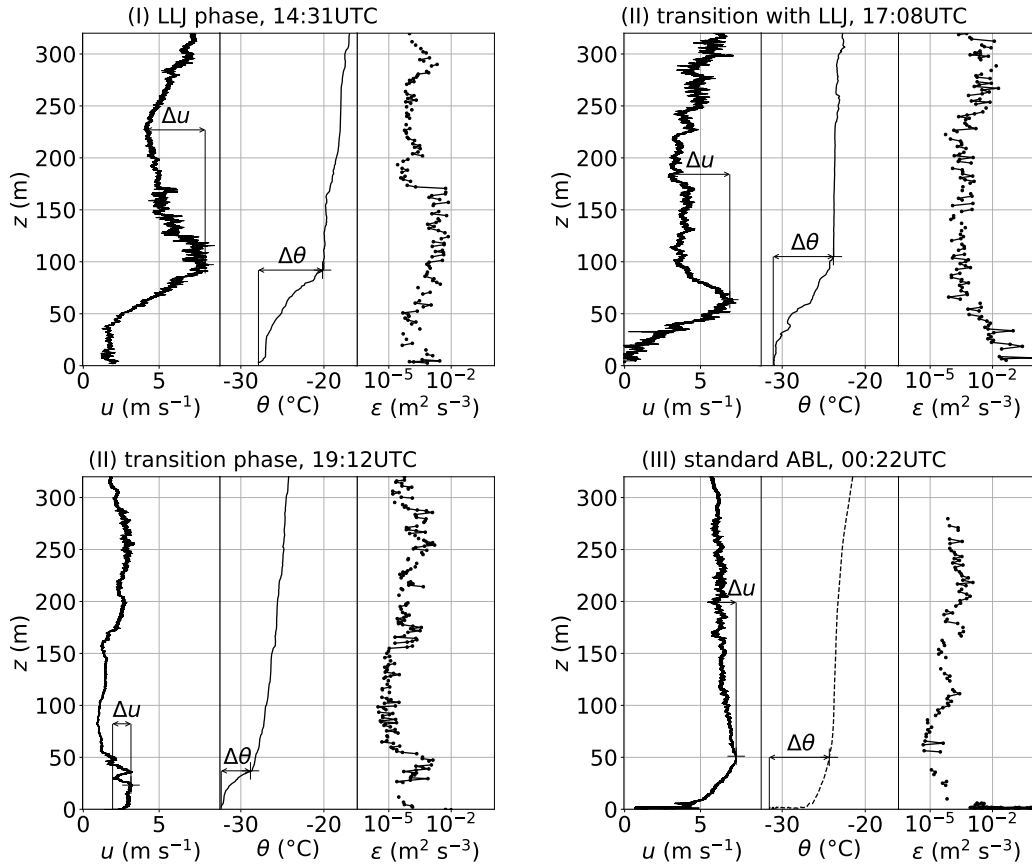


**Figure 4.** Example vertical profiles for each phase: wind velocity  $u$  with the definition of LLJ strength  $\Delta u$  and LLJ height  $z_{LLJ}$ , potential temperature  $\theta$  with the temperature inversion strength  $\Delta\theta$  and inversion height  $z_i$  and dissipation rate  $\epsilon$ . For the transition phase, one profile with and one profile without LLJ is shown.

more clearly with the inversion height ( $R = 0.64$ ).  $Ri_b$  is increased in the transition period and around  $Ri=1$  (weak turbulence) for the other two periods. Energy dissipation  $\epsilon$  in the LLJ period is one order of magnitude higher than in phases II and III and shows much more variability. The turbulent fluxes of heat  $H$  and momentum  $\tau_u$  show increased values and variability and individual events with high flux magnitude in the LLJ period, compared to low fluxes in the transition and standard ABL phase. The LLJ, as observed at 17:04 UTC coincides with a short period of weak upward-oriented momentum fluxes and downward heat fluxes.

## 4.2 Normalized vertical profiles

Each of the three periods introduced in Sect. 4.1 features a distinct vertical structure of thermodynamic and turbulence parameters. For each of the three periods, Fig. 6 shows normalized vertical profiles. Whereas the height is normalized with  $z_i$ ,  $u$  is

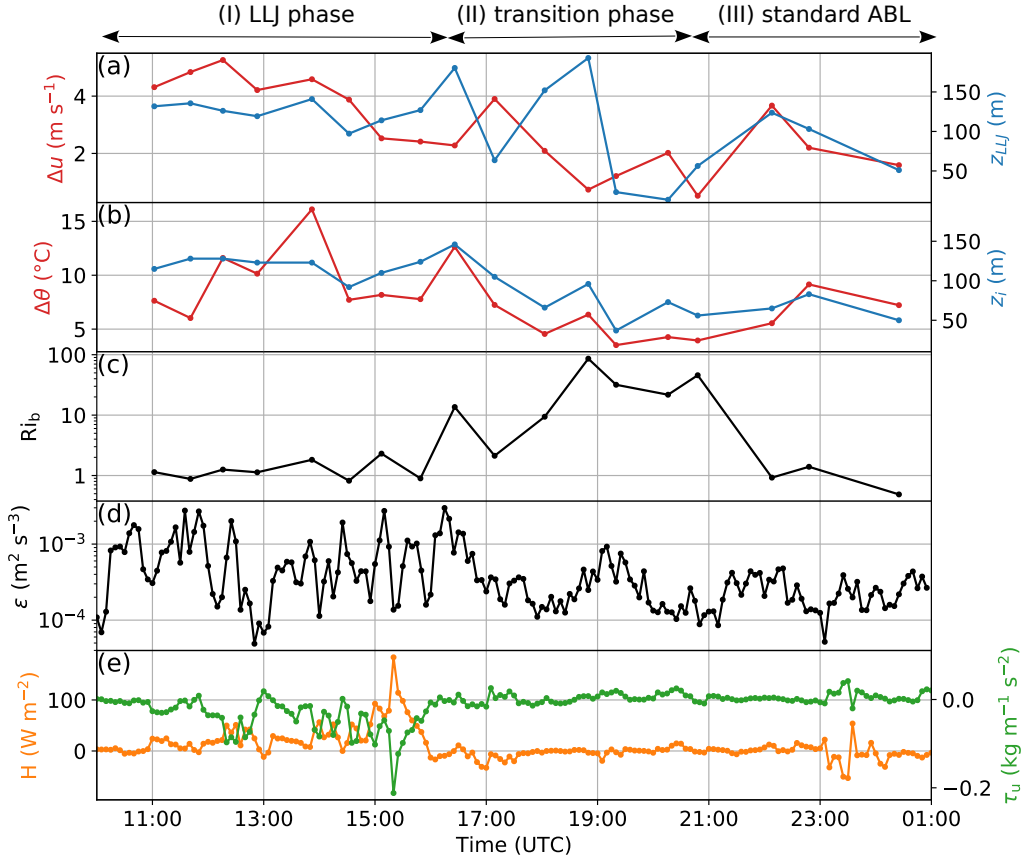


**Figure 5.** Temporal development of (a) the LLJ parameters strength  $\Delta u$  and height  $z_{LLJ}$ , (b) the temperature inversion strength  $\Delta\theta$  and height  $z_i$ , (c) bulk Richardson number  $Ri_b$  (between surface and  $z_i$ ), (d) dissipation rate  $\varepsilon$  at 65 m (5 min averages) and (e) turbulent fluxes  $H$  and  $\tau_u$  at 65 m (calculated every 5 min for a 30 min period).

normalized with  $u_{\max}$  (below 300 m), and  $\theta$  and  $q$  are normalized with their values at  $z_i$ . The box plots are assigned to height intervals and include median values for each profile within the respective period. The wind velocity profile shows a characteristic shape for the LLJ period and the standard stable ABL period, with low variability within the profiles. The transition phase exhibits much higher variability, and wind velocity increases with height. The  $\theta$  and  $q$  profiles are similar for all phases, with the lowest variability below  $z_i$  for the LLJ period. In each period, there is a turbulence maximum in  $\varepsilon$  close to the surface, which indicates surface-driven turbulence for all cases. In relation to the wind profile, the vertical turbulence profile is different for each period and will be discussed in more detail.

In the LLJ period, the average  $\varepsilon$  structure has a characteristic shape with two local maxima: near the surface and at  $z/z_i \approx 1.5$  with reduced values around  $z_i$  itself. A local minimum of  $\varepsilon$  at  $z/z_i \approx 0.3$  suggests decoupling of the LLJ from the surface. In the transition period, the average  $u$  profile is almost height-constant but shows high internal variability. The  $\varepsilon$  profile is

highly variable with height without any characteristic structure. The only common features are minimum values around  $z_i$  and maximum values close to the surface.

205 The last period is characterized by a gradual increase of the normalized velocity from the surface up to  $z_i$  followed by a slight decrease above. Turbulence shows comparable high values only close to the surface with a clear minimum around  $z_i$  where values close to the resolution limit are observed. The low variability within the profiles results partly from only two profiles with turbulence measurements in this phase. The profiles of  $Ri_g$  generally match the  $\varepsilon$  profiles with low  $Ri_g$  correlating with high  $\varepsilon$  but generally showing a high variability.

210 These normalized profiles show that the presence of an LLJ enhances turbulent mixing directly above and below the jet maximum compared to a stable ABL without an LLJ. The turbulence increase is more pronounced above the jet core. However, a stably stratified region close to the surface with height-constant wind speeds decouples the LLJ from the surface. The enhanced turbulent mixing by the LLJ might be important for the vertical mixing of advected long-range transported tracers.

## 5 Summary and discussion

215 This study presents the observation of an LLJ based on tethered balloon measurements in the late winter central Arctic in March 2018 in northeast Greenland at the Villum Research Station/ Station Nord. The measurements span a 15-h period with a transition from a stable ABL with a prominent LLJ to a classically stable nocturnal ABL without an LLJ. The observations include measurements of mean standard meteorological measurements as well as turbulence measurements from the ground to well above the ABL (typically 300 m). The balloon observations were supported by continuous turbulence measurements on a mast at 65 m height – corresponding to the lower part of the LLJ.

220 During the LLJ phase, observations indicate increased turbulence (increased local dissipation rates) within the LLJ, but the increased turbulence does not reach the surface. Only during the transition phase to a more classical boundary layer structure do these increased turbulence intensities also reach the surface, allowing thorough mixing to occur. These observations lead to the hypothesis that within an LLJ, a passive tracer can be 'trapped' and transported over a long distance, without vertical mixing beyond the LLJ boundaries greatly reducing the tracer concentration. Only the dissolution of the LLJ can finally lead  
225 to an increased concentration also at the ground.

An accompanying analytical model study (Hellmuth et al., 2023) shows that LLJs may impact aerosol formation and evolution under Arctic conditions. However, the one-dimensional analytical LLJ model revealed difficulties in the reproduction of the observed LLJ wind peak (underestimation of the sharpness of the observed vertical wind velocity), which leads to a misprediction of the shear-induced contribution to the TKE budget. As a consequence, the TKE production at the LLJ level  
230 is underestimated. The removal of this shortcoming would require the consideration of momentum advection, baroclinity, and terrain-induced cold-air flow. Nevertheless, within the framework of this conceptual study, we demonstrate that an LLJ can effectively promote the horizontal transport of a passive tracer released close to the ground. This result, in turn, suggests that a LLJ may have a significant impact on both in-situ and ex-situ aerosol formation and evolution under Arctic conditions. In fu-

ture research, the simulation of the intrinsically three-dimensional nature of this phenomenon with a more sophisticated model  
235 requires further investigation through appropriate observations of the parameters involved, including vertical profiling.

*Data availability.* The observational data for this manuscript are publicly available (Egerer et al., 2019b).

*Author contributions.* UE and HS performed the balloon measurements and processed and analyzed the data. LLS contributed the meteorological mast measurements. OH contributed to the data evaluation and discussion. All co-authors contributed to drafting the manuscript.

*Competing interests.* The authors declare that they have no conflict of interest.

240 *Acknowledgements.* We gratefully acknowledge the funding by the Deutsche Forschungsgemeinschaft (DFG, German Research Foundation)  
- project number 268020496 - TRR 172, within the Transregional Collaborative Research Center “Arctic Amplification: Climate Relevant  
Atmospheric and Surface Processes, and Feedback Mechanisms (AC)<sup>3</sup>” in sub-project A02. We acknowledge the essential help of Andreas  
Herber, Jens Voigtländer, Frank Stratmann, PAMARCMiP scientists and the crew of Station Nord and Villum Research Station during the  
balloon operations. Sven-Erik Gryning provided and advised us on ceilometer and wind lidar data at VRS. We wish to thank Andreas  
245 Massling, Daniel Charles Thomas, and Jakob Boyd Pernov for discussing VRS data.

## References

- Abarbanel, H. D. I., Holm, D. D., Marsden, J. E., and Ratiu, T.: Richardson number criterion for the nonlinear stability of three-dimensional stratified flow, *Phys. Rev. Lett.*, 52, 2352–2355, <https://doi.org/10.1103/PhysRevLett.52.2352>, 1984.
- Algarra, I., Eiras-Barca, J., Miguez-Macho, G., Nieto, R., and Gimeno, L.: On the assessment of the moisture transport by the Great Plains low-level jet, *Earth. Syst. Dynam.*, 10, 107–119, <https://doi.org/10.5194/esd-10-107-2019>, 2019.
- Andreas, E. L., Claffey, K. J., and Makshtas, A. P.: Low-level atmospheric jets and inversions over the western Weddell Sea, *Boundary-Layer Meteorology*, 97, 459–486, <https://doi.org/10.1023/A:1002793831076>, 2000.
- Banta, R. M., Pichugina, Y. L., and Brewer, W. A.: Turbulent Velocity-Variance Profiles in the Stable Boundary Layer Generated by a Nocturnal Low-Level Jet, *Journal of the Atmospheric Sciences*, 63, 2700–2719, <https://doi.org/10.1175/JAS3776.1>, 2006.
- Blackadar, A. K.: Boundary Layer Wind Maxima and Their Significance for the Growth of Nocturnal Inversions, *Bulletin of the American Meteorological Society*, 38, 283–290, <https://doi.org/10.1175/1520-0477-38.5.283>, 1957.
- Chechin, D. G. and Lüpkes, C.: Baroclinic low-level jets in Arctic marine cold-air outbreaks, *IOP Conference Series: Earth and Environmental Science*, 231, 012 011, <https://doi.org/10.1088/1755-1315/231/1/012011>, 2019.
- Egerer, U., Gottschalk, M., Siebert, H., Ehrlich, A., and Wendisch, M.: The new BELUGA setup for collocated turbulence and radiation measurements using a tethered balloon: first applications in the cloudy Arctic boundary layer, *Atmospheric Measurement Techniques*, 12, 4019–4038, <https://doi.org/10.5194/amt-12-4019-2019>, 2019a.
- Egerer, U., Siebert, H., Voigtländer, J., and Gottschalk, M.: Tethered balloon-borne measurements of turbulence and radiation during the Arctic field campaign PAMARCMiP in March/ April 2018, <https://doi.org/10.1594/PANGAEA.900240>, 2019b.
- Guest, P., Persson, P. O. G., Wang, S., Jordan, M., Jin, Y., Blomquist, B., and Fairall, C.: Low-Level Baroclinic Jets Over the New Arctic Ocean, *Journal of Geophysical Research: Oceans*, 123, 4074–4091, <https://doi.org/https://doi.org/10.1002/2018JC013778>, 2018.
- Hellmuth, O., Egerer, U., Siebert, H., and Sørensen, L. L.: PAMARCMiP Contribution: An analytic model companion based on observations: The role of low-level jets in the advection of passive tracers in the high Arctic, *Tech. rep.*, <https://doi.org/10.5281/zenodo.7689308>, 2023.
- Jakobson, L., Vihma, T., Jakobson, E., Palo, T., Männik, A., and Jaagus, J.: Low-level jet characteristics over the Arctic Ocean in spring and summer, *Atmospheric Chemistry and Physics*, 13, 11 089–11 099, <https://doi.org/10.5194/acp-13-11089-2013>, 2013.
- López-García, V., Neely, R. R., Dahlke, S., and Brooks, I. M.: Low-level jets over the Arctic Ocean during MOSAiC, *Elementa: Science of the Anthropocene*, 10, 2022.
- Mahrt, L.: Vertical structure and turbulence in the very stable boundary layer, *J. Atmos. Sci.*, 42, 2333–2349, 1985.
- Mahrt, L.: Stratified Atmospheric Boundary Layers, *Bound.-Layer Meteor.*, 90, 375 – 396, 1999.
- Miles, J. W.: On the stability of heterogeneous shear flows, *Journal of Fluid Mechanics*, 10, 496–508, <https://doi.org/10.1017/S0022112061000305>, 1961.
- Siebert, H., Lehmann, K., and Wendisch, M.: Observations of small scale turbulence and energy dissipation rates in the cloudy boundary layer., *J. Atmos. Sci.*, 63, 1451 – 1466, 2006.
- Smedman, A.-S., Tjernström, M., and Högrström, U.: Analysis of the turbulence structure of a marine Low-Level Jet, *Bound.-Layer Meteor.*, 66, 195–126, 1993.
- Stensrud, D. J.: Importance of Low-Level Jets to Climate: A Review, *J. Climate*, 9, 1698–1711, 1996.
- Tuononen, M., Sinclair, V. A., and Vihma, T.: A climatology of low-level jets in the mid-latitudes and polar regions of the Northern Hemisphere, *Atmospheric Science Letters*, 16, 492–499, <https://doi.org/https://doi.org/10.1002/asl.587>, 2015.

- Vihma, T., Kilpeläinen, T., Manninen, M., Sjöblom, A., Jakobson, E., Palo, T., Jaagus, J., and Maturilli, M.: Characteristics of Temperature and Humidity Inversions and Low-Level Jets over Svalbard Fjords in Spring, *Advances in Meteorology*, 2011, 1–14, 285 <https://doi.org/10.1155/2011/486807>, 2011.
- Wilczak, J. M., Oncley, S. P., and Stage, S. A.: Sonic anemometer tilt correction algorithms, *Boundary-Layer Meteorology*, 99, 127–150, <https://doi.org/10.1023/A:1018966204465>, 2001.
- Wyngaard, J. C.: *Turbulence in the atmosphere*, Cambridge University Press, <https://doi.org/10.1017/CBO9780511840524>, 2010.

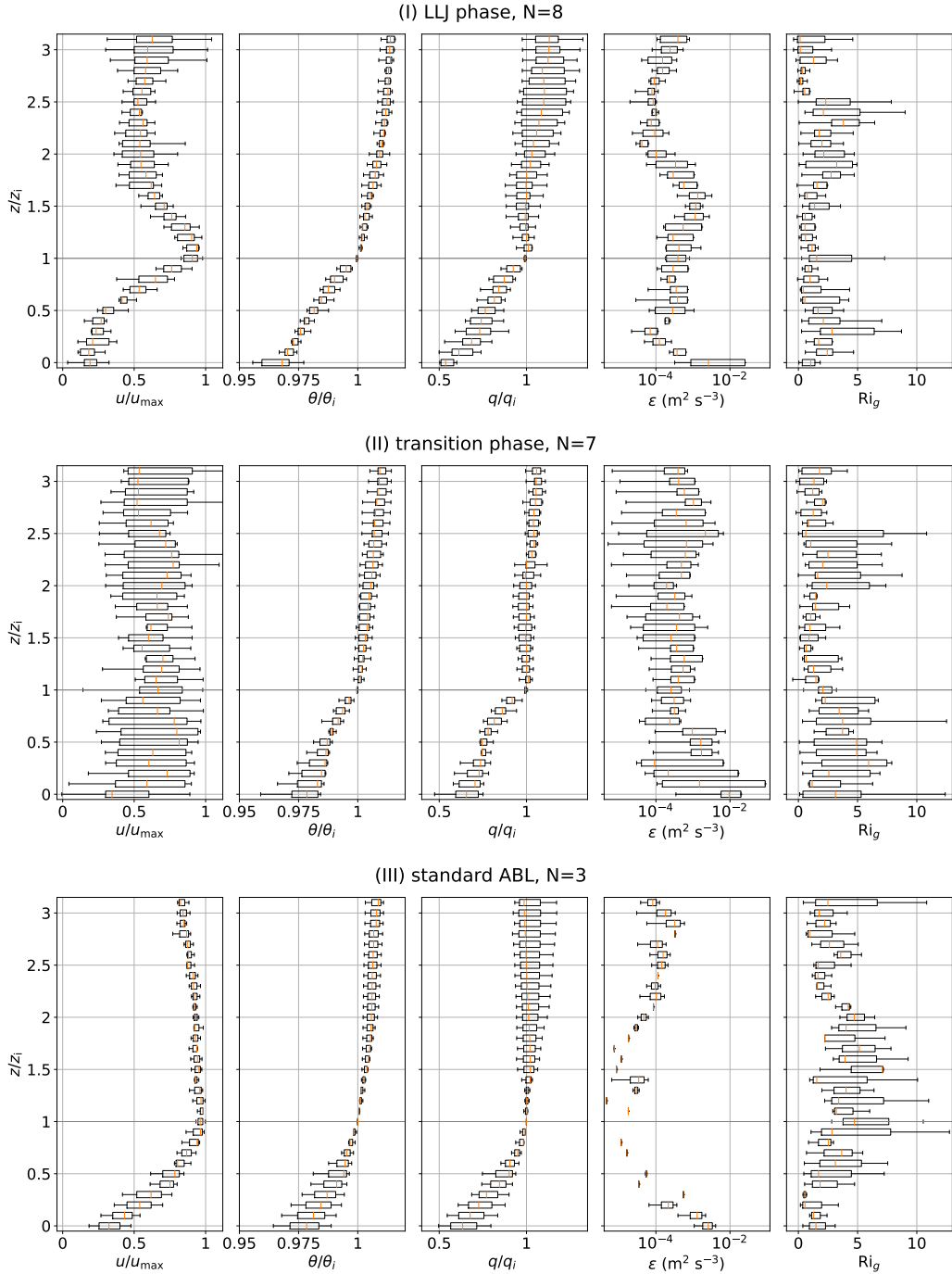


**Figure 6.** Normalized vertical profiles of  $u$ ,  $\theta$ ,  $\varepsilon$ ,  $Ri_g$  and  $q$  for phase I (with LLJ, top), phase II (transition, center) and phase III (profiles without LLJ, bottom). The box plots show variations within the individual  $N$  profiles in each phase. The height  $z$  is normalized with the temperature inversion base height  $z_i$ . The wind velocity is normalized with  $u_{\max}$  ( $u_{\text{LLJ}}$  or maximum  $u$  below 300 m). The quantities  $\theta$  and  $q$  are normalized with their value at  $z_i$ . The boxes include the lower and upper quartile values of the data, with the orange line at the median.